the interstitial waters is consistent with the high methane level, as sulfate reduction precedes methane formation during diagenesis of organic matter (see "Organic Geochemistry," p. 30). High sulfate levels probably represent the original sulfate concentration that has not been used by bacteria, possibly because of the lack of enough metabolizable organic matter below lithostratigraphic Unit I (see "Lithostratigraphy," p. 4). In addition, the comparably low sedimentation rate (see "Age Models and Sedimentation Rates," p. 25) may have allowed significant amounts of sulfate to diffuse downward and replenish the sulfate reservoir used by bacteria.

Ammonium (NH_4^+) concentrations remain almost constant down to 53.20 mbsf, then increase to a maximum of 5.90 mM at 147.90 mbsf (Fig. F30). Below 53.20 mbsf, ammonium values steadily decrease down to 431.40 mbsf and then remain constant to the bottom. An increase of the ammonium concentration reflects the intensive bacterial degradation of organic matter, whereas a decrease indicates the results of ion exchange reactions on the surfaces of clay minerals and/or the subsequent incorporation into interlayers of diagenetically formed clay minerals (Gieskes, 1981).

The phosphate (HPO_4^{2-}) concentrations decrease with depth down to 305.90 mbsf (Fig. F30). Below 305.90 mbsf, the concentrations are relatively constant, but decrease slowly with depth. This trend indicates rather strong first-order removal, suggesting a diagenetic uptake of dissolved phosphate, most likely into sedimentary mineral phases.

Calcium, Magnesium, and Strontium

Calcium (Ca^{2+}) concentrations initially decrease from a subsurface value of 4.9 to 3.5 mM at ~100 mbsf, because of carbonate precipitation resulting from the buildup of alkalinity during sulfate reduction (Fig. F30). The absence of SO_4^{2-}, high alkalinity, and high Mg^{2+}/Ca^{2+} ratios may provide a favorable geochemical environment for dolomite formation (Baker and Kastner, 1981). Between ~300 and ~500 mbsf, Ca^{2+} concentrations increase strongly up to 18.9 mM.

The profile of magnesium (Mg^{2+}) shows high concentrations in the upper 25 mbsf of Hole 1122A (Fig. F30). High Mg^{2+} values have been observed almost ubiquitously in anoxic environments and are thought to result from the desorption of Mg^{2+} from solid phases in rapidly accumulating sediments (Gieskes et al., 1982). From ~25 mbsf, Mg^{2+} decreases with depth down to 272.70 mbsf, which indicates precipitation of dolomite. Between 300 and 450 mbsf, a distinct Mg^{2+} anomaly occurs. Concentration variations of these elements may be influenced by diagenetic controls within this lithologic unit or diffusive transport by fluid movement within this interval.

Dissolved strontium (Sr^{2+}) concentrations increase slightly from 75 µM at 5.90 mbsf to 173 µM at 243.70 mbsf and then increase rapidly to a maximum of 466 µM at 370.40 mbsf (Fig. F30). The Sr^{2+} values remain relatively constant throughout the lower part of Hole 1122C. Increasing strontium concentrations in interstitial waters may originate either from the recrystallization of biogenic carbonate (the associated strontium concentration decrease in the recrystallizing carbonate may be more than one order of magnitude) or the alteration of tephras. The maximum Sr^{2+} concentrations occur at the same level as the Mg^{2+} maximum, which indicates an additional input of these two elements into this interval. The change of the Sr^{2+} gradient at ~460 mbsf coincides

with the lithologic boundary between Subunit IIA and IIB (see "Lithostratigraphy," p. 4).

Dissolved Silica, Potassium, and Lithium

Dissolved silica (H_4SiO_4) concentrations increase gradually from 575 µM at 5.90 mbsf to 803 µM at 591.80 mbsf (Fig. F30). The dissolved silica increases indicate progressive diatom dissolution. However, the relatively large scatter of the silica data may reflect the fairly heterogeneous sediment composition.

Potassium (K^+) concentrations decrease from 10.6 mM at the subsurface to 6.5 mM at the bottom of the core (Fig. F30). This indicates large-scale removal of K^+ into clay minerals that are forming within the sediments.

The dissolved lithium (Li^+) concentrations increase slightly from 18 µM at 5.90 mbsf to 87 µM at 399.50 mbsf and increase steeply to a maximum of 231 µM at the bottom of the hole (Fig. F30). Because the Li^+ concentration is related to the biogenic silica content (Gieskes, 1981), the general increase indicates release of Li^+ during diatom dissolution and silica transformation. The abrupt increase in Li^+ concentration in the lower part of the hole, which corresponds to the boundary between Subunits IIA and IIB (see "Lithostratigraphy," p. 4), reflects an additional source of Li^+ into the pore fluids, because the dissolved silica concentrations decrease in this interval.

Summary of Interstitial Water Results

The primary controlling factor on the interstitial-water chemistry at Site 1122 is sulfate reduction and methanogenesis, which governs alkalinity, phosphate, and ammonium concentration. In contrast to the complete utilization of sulfate in the upper part of the core, the increased sulfate levels in the middle of the section represent the original sulfate concentrations during sediment deposition, possibly preserved because of a lack of sufficient metabolizable organic matter and low sedimentation rates. Other important chemical profiles are magnesium and calcium concentrations, from which we may deduce the lateral transport of magnesium-rich fluid during the dissolution of carbonate. The general chemical zonations of interstitial waters at Site 1122 correspond to those of lithostratigraphic units and paleontological age divisions. In particular, note the sharp reduction of methane at 260 mbsf, which coincides with the base of the highly pyritized turbidites of the mud-wave sequence.

ORGANIC GEOCHEMISTRY

Volatile Hydrocarbons

As part of the shipboard safety and pollution-prevention monitoring program, hydrocarbon gases were analyzed for each core of Hole 1122A and each core below 60 mbsf of Hole 1122C by the headspace technique. Gas pockets were not encountered. The headspace methane concentrations increase rapidly below the seafloor (Fig. F31). In contrast to Site 1119 (see "Organic Geochemistry," p. 24, in the "Site 1119" chapter), there is no well-defined concentration maximum in the section, but headspace methane concentrations of the sediments between 15

F31. Headspace methane concentrations in sediments from Holes 1122A and 1122C, p. 74.

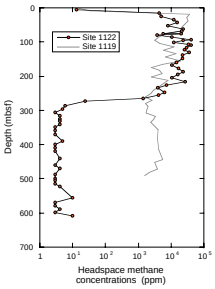

and 265 mbsf are much higher than in the uppermost sample and in the sediments below. The variation in this section (1,000–42,000 ppm) may reflect different sediment properties and/or different amounts of metabolizable organic matter in the methane-releasing sediments and, thus, changes in the sedimentary composition. The elevated methane concentrations are corroborated by low sulfate concentrations (see "Inorganic Geochemistry," p. 27). Below 265 mbsf, methane concentrations decrease suddenly by two orders of magnitude and are uniformly low down to the bottom of the hole. This distinct change matches the transition from lithostratigraphic Subunit IC to Subunit IB at 262 mbsf (see "Lithostratigraphy," p. 4), and may be a result of changes in the amount or type of organic matter. However, clear corresponding evidence of these changes cannot be found in the elemental composition (see "Carbonate and Organic Carbon," p. 31).

Carbonate and Organic Carbon

The abundance of total, inorganic, and organic carbon and of calcium carbonate in sediments from Holes 1122A and 1122B is summarized in Table T14 (also in ASCII format). Random sampling of all lithologies was performed for carbonate analysis, and one sample per core was analyzed for organic carbon.

Carbonate contents are highly variable throughout the section and lie in the range from 0.1 to 76.5 wt% (Fig. F32). There is no clear correlation with depth, age, or lithology. Because of the obvious variation in the sedimentary composition, particularly the intercalated turbidites in the hemipelagic sediments, this may be an artifact of random sampling. Nevertheless, in the upper part of the section between 0 and 140 mbsf, with exception of the section from 60 to 80 mbsf (lithostratigraphic Subunits IA and IB) and between 300 and 420 mbsf, carbonate contents are lower on average than in the rest of the section.

Sediments at Site 1122 average 0.24 wt% organic carbon (Fig. F33), which is lower than the average for deep-sea sediments of 0.3% compiled by McIver (1975) from data of DSDP Legs 1 through 33. There is no clear correlation with depth, age, or lithology, though in the deeper part of the hole concentrations seem to decrease with increasing depth. Despite the high sedimentation rate, low organic carbon concentrations are probably a consequence of organic-matter degradation caused by the long exposure to an oxic water column.

Organic Matter Source Characterization

Atomic organic carbon/nitrogen values were calculated for Site 1122 samples using TOC and total nitrogen concentrations to help identify the origin of the organic matter. The ratios vary from 0.2 to 25.9 with an average of 4.2 (Table T14). These low ratios are not accurate indicators of organic matter source. They may be an artifact of the low organic carbon content, combined with the tendency of clay minerals to adsorb ammonium ions generated during degradation of organic matter (Müller, 1977). This interpretation is supported by unrealistically low atomic $[C/N]_a$ ratios below 4.0 for organic carbon–poor samples (<0.2 wt%).

Rock-Eval analyses were not made because of low organic carbon contents (see "Organic Geochemistry," p. 22, in the "Explanatory Notes" chapter).

T14. Organic chemistry data, p. 141.

F32. Carbonate contents in sediments from Holes 1122A and 1122C, p. 75.

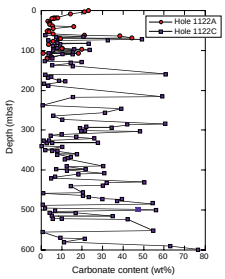

F33. Organic carbon contents in sediments from Holes 1122A and 1122C, p. 76.

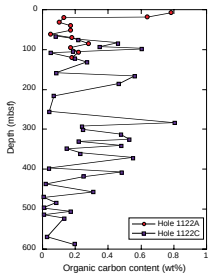

PHYSICAL PROPERTIES

Index Properties

Index properties measurements were made at a resolution of one sample every two sections in the cores from Holes 1122A and 1122C. Index properties were determined by a gravimetric method (see "Physical Properties," p. 24, in the "Explanatory Notes" chapter). Values of measured index properties (void ratio, porosity, water content, bulk density, and grain density) are presented in Table T15 (also in ASCII format). The properties measured from Holes 1122A and 1122C show cyclic variations downcore resulting from compositional variations typical of turbidite sequences (Figs. F34, F35). In the upper 500 mbsf, there is no apparent change in trend for any of the variables measured. Below 500 mbsf, the index properties show gradual downhole changes in trend, presumably from the effects of increased overburden.

Multisensor Track Measurements

The shipboard physical properties program at Site 1122 included nondestructive measurements of bulk density, magnetic susceptibility, and natural gamma-ray activity on whole sections of all cores using the MST (Figs. F36, F37). Magnetic susceptibility was measured at 4-cm intervals and at high sensitivity (4-s measurement time) in all Site 1122 holes. High-amplitude fluctuations of magnetic susceptibility in Hole 1122A and in the upper part (<110 mbsf) of Hole 1122C are associated with turbidite sequences. The presence of low magnetic susceptibility values with little variation below 110 mbsf in Hole 1122C is probably a result of low recovery of sands by XCB coring. Thus, there is a tendency for recovered core material to be clay rich. Natural gamma radiation was measured with a 15-s count every 14 cm in Holes 1122A and 1122C. Natural gamma radiation ranges from 15 to 42 counts/s. Variations occurring downcore reflect changes in mineral composition between sandy and clayey layers in the turbidite sequence. High values of natural gamma radiation give an indication of the relative abundance of clay. Low natural gamma radiation values shown in Hole 1122A are correlated with low magnetic susceptibility, indicating a possible increase in sand content. Gamma-ray attenuation porosity evaluator bulk density measurements were made at 4-cm intervals at all Site 1122 holes. The GRAPE density data exhibit fluctuations that tend to vary in direction, thickness, and intensity with those observed in the natural gamma radiation record; these fluctuations seem to correspond to variations in the occurrence of sandy and clay-rich sediment layers. A comparison of GRAPE density with the wet-bulk density determined from discrete samples shows a general agreement except in the uppermost part of the hole (Fig. F38).

Shear Strength

Measurements of shear strength, using a mechanical vane, were made on split cores from Holes 1122A and 1122C (Fig. F39). Samples were generally taken in fine-grained sediments at a resolution of one per section. No samples were taken from XCB cores. The shear strength measurements show relatively low values, except for peaks just above 35 and 65 mbsf in Hole 1122A and 42, 69, and 92 mbsf in Hole 1122C. These peaks indicate clay-rich intervals (see "Lithostratigraphy," p. 4).

T15. List of index properties measurements, p. 144.

F34. Index properties measurements from cores from Hole 1122A, p. 77.

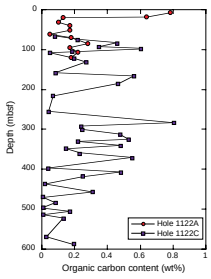

F35. Index properties measured from cores from Hole 1122C, p. 78.

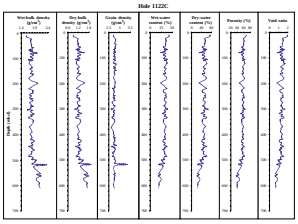

F36. MST track measurements from Hole 1122A, p. 79.

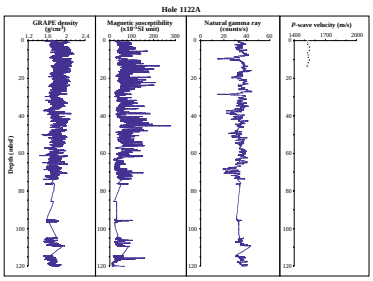

F37. MST measurements from Hole 1122C, p. 80.

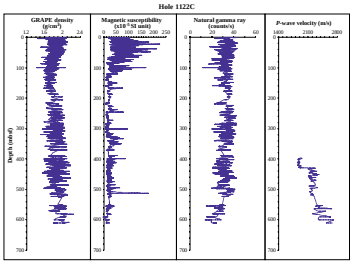

Shear strength values range from 5 to 60 kPa (maximum value of 57.15 kPa at 65 mbsf in Hole 1122A and 60.525 kPa at 91 mbsf in Hole 1122C). Low values may be associated with the presence of sand-rich intervals (see "Lithostratigraphy," p. 4). An indication of the consolidation characteristics of the sediments was made by using the classical relationship between shear strength and sedimentary overburden pressure (see "Physical Properties," p. 22, in the "Site 1121" chapter). The consolidation data from Site 1122 are similar in character to those from Site 1119 where cyclic variations also occur. Underconsolidation exists downhole as a result of rapid, increasingly sandy deposition. It is likely that the sediment is still undelrconsolidated, that is, still in the process of expelling pore water. The fact that water content and porosity remain relatively constant throughout the section supports this hypothesis.

F38. Density measurements in Hole 122C, p. 81.

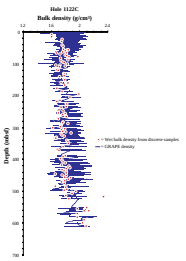

F39. Distribution of shear strength in cores, p. 82.

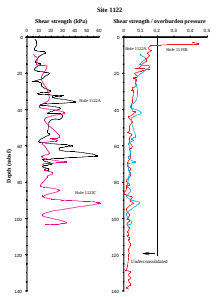

Compressional-Wave Velocity

Compressional-wave (*P*-wave) velocity was measured parallel to the core axis on split cores from Site 1122. Because the sediment cracked when the transducers of the Digital Sound Velocimeter were inserted into the sandy turbidite sediment, the measurements were only taken in the upper 20 mbsf of Hole 1122A. Values range from 1527 m/s to 1547 m/s. Below 390 mbsf in Hole 1122C, sediments were more tightly compacted, and the Hamilton frame velocimeter was used to measure sound propagation perpendicular to the sediment. A sharp increase in *P*-wave velocity from 1800 to 2000 m/s occurred around 429 mbsf between Sections 181-1122C-48X-2 and 48X-3, indicating a distinct lithologic horizon.

DOWNHOLE MEASUREMENTS

Logging Operations

Logging was attempted in Hole 1122C but was unsuccessful because of adverse weather and poor hole conditions. We planned to run one pass of the triple combination, two passes of the FMS-sonic, and then a single pass of the GHMT (for abbreviations and explanation of the tool strings see "Downhole Measurements," p. 29, in the "Explanatory Notes" chapter). Logging operations began at 0700 hr on 11 September 1998 and were terminated at 1330 hr on the same day.

After coring the hole to 627.4 mbsf, the BHA was raised to 83.12 mbsf, in preparation for logging. Raising the BHA was, however, problematic, and resulted in substantial infilling at the base of the hole (see "Operations," p. 3). The heave on the ship (>6 m) was too great to allow use of the wireline heave compensator (WHC). Because of this, it was decided not to open the calipers on the FMS and lithodensity tools, in case the excessive heave ripped them off.

The triple combination was lowered to the base of the pipe, but could not pass completely into the open hole because of an obstruction at 95 mbsf, ~12 m below the BHA. Weather at the time was poor, with 3.5-m seas, 6-m swells, and 37-kt winds. After trying unsuccessfully for 35 min to break through the obstruction, the triple combination was pulled back into the drill string. An attempt was made to pull up the BHA, but it had become stuck. At this point the triple combination was brought back up to the rig floor and disassembled.

A revised logging plan was considered, consisting of a wiper trip with the drill string to clean out the hole, followed by a single pass of a shorter tool string. The new tool string would consist of the gamma-ray, sonic, resistivity, and temperature tools. If this pass had been successful, a run of the GHMT would have followed. However, by this time weather conditions had deteriorated with the swells increasing to a maximum of 10 m and the winds to 45 kt. The forecast was for deteriorating weather. These conditions constituted a danger to the drill string and a risk to the tools. Therefore, it was decided to abandon logging operations at Hole 1122C. It took a further 2 hr to free the BHA from the hole.

REFERENCES

Baker, P.A., and Kastner, M., 1981. Constraints on the formation of sedimentary dolomite. *Science,* 213:215–216.

Baksi, A.K., 1995. Fine tuning the radiometrically derived geomagnetic polarity time scale (GPTS) for 0–10 Ma. *Geophys. Res. Lett.,* 22:457–460.

Berggren, W.A., Kent, D.V., Swisher, C.C., III, and Aubry, M.-P., 1995. A revised Cenozoic geochronology and chronostratigraphy. *In* Berggren, W.A., Kent, D.V., Aubry, M.-P., and Hardenbol, J. (Eds.), *Geochronology, Time Scales and Global Stratigraphic Correlation*. Spec. Publ.—Soc. Econ. Paleontol. Mineral. (Soc. Sediment. Geol.), 54:129–212.

Brew, D.S., 1995. Mud waves at Deep Sea Drilling Project Site 603, US Atlantic lower continental rise. *Geo-Mar. Lett.,*15:92–98.

Cande, S.C., and Kent, D.V., 1995. Revised calibration of the geomagnetic polarity timescale for the Late Cretaceous and Cenozoic. *J. Geophys. Res.,* 100:6093–6095.

Carter, L., and Carter, R.M., 1988. Late Quaternary development of left bank dominant levees in the Bounty Trough, New Zealand. *Mar. Geol.,* 78:185–197.

————, 1993. Sedimentary evolution of the Bounty Trough: a Cretaceous rift basin, southwestern Pacific Ocean. *In* Ballance, P.F. (Ed.), *Sedimentary Basins of the World—South Pacific:* Amsterdam (Elsevier), 51–67.

Carter, L., Carter, R.M., Nelson, C.S, Fulthorpe, C.S., and Neil, H.L., 1990. Evolution of Pliocene to Recent abyssal sediment waves on Bounty Channel levees, New Zealand. *Mar. Geol.,* 95:97–109.

Carter, L., Nelson, C.S., Neil, H.L., and Froggatt, P.C., 1995. Correlation, dispersal, and preservation of the Kawakawa Tephra and other late Quaternary tephra layers in the Southwest Pacific Ocean. *N. Z. J. Geol. Geophys.,* 38:29–46.

Carter, R.M., and Carter, L., 1987. The Bounty Channel system: a 55-million-year-old sediment conduit to the deep sea, Southwest Pacific Ocean. *Geo-Mar. Lett.,* 7:183–190.

————, 1992. Seismic imaging of Pleistocene deep-sea cyclothems: implications for sequence stratigraphy. *Terra Nova,* 4:682–692.

————, 1996. The abyssal Bounty Fan and lower Bounty Channel: evolution of a rifted-margin sedimentary system. *Mar. Geol.,* 130:182–202.

Carter, R.M., Carter, L., and Davy, B., 1994. Seismic stratigraphy of the Bounty Trough, Southwest Pacific Ocean. *Mar. Pet. Geol.,* 11:79–93.

Damuth, J.E., 1979. Migrating sediment waves created by turbidity currents in the northern South China Basin. *Geology,* 7:520–523.

Davey, B.W., 1993. The Bounty Trough: basement structure influences on sedimentary basin evolution. *In* Ballance, P.F. (Ed.), *Sedimentary Basins of the World—South Pacific:* Amsterdam (Elsevier), 69–92.

de Kaenel, E., and Villa, G., 1996. Oligocene–Miocene calcareous nannofossils biostratigraphy and paleoecology from the Iberia Abyssal Plain. *In* Whitmarsh, R.B., Sawyer, D.S., Klaus, A., and Masson, D.G. (Eds.), *Proc. ODP, Sci. Results,* 149: College Station, TX (Ocean Drilling Program), 79–145.

Fenner, J., Carter, L., and Stewart, R., 1992. Late Quaternary paleoclimatic and paleoceanographic change over northern Chatham Rise, New Zealand. *Mar. Geol.,* 108:383–404.

Gartner, S., 1992. Miocene nannofossil chronology in the North Atlantic, DSDP Site 608. *Mar. Micropaleontol.,* 18:307–331.

Gieskes, J.M., 1974. Interstitial water studies, Leg 25. *In* Simpson, E.S.W., Schlich, R., et al., *Init. Repts. DSDP,* 25: Washington (U.S. Govt. Printing Office), 361–394.

————, 1981. Deep-sea drilling interstitial water studies: implications for chemical alteration of the oceanic crust, layers I and II. *In* Warme, J.E., Douglas, R.G., and Winterer, E.L. (Eds.), *The Deep Sea Drilling Project: A Decade of Progress*. Spec. Publ.—Soc. Econ. Paleontol. Mineral., 32:149–167.

Gieskes, J.M., Elderfield, H., Lawrence, J.R., Johnson, J., Meyers, B., and Campbell, A., 1982. Geochemistry of interstitial waters and sediments, Leg 64, Gulf of California. *In* Curray, J.R., Moore, D.G., et al., *Init. Repts. DSDP,* 64 (Pt. 2): Washington (U.S. Govt. Printing Office), 675–694.

Gradstein, F.M., Fearon, J.M., and Huang, Z., 1989. BURSUB and DEPOR version 3.50—two FORTRAN 77 programs for porosity and subsidence analysis. *Open-File Rep.—Geol. Surv. Can.,* 1283:1–10.

Griggs, G.B., Carter, L., and Kennett, J.P., and Carter, R.M., 1983. Late Quaternary marine stratigraphy southeast of New Zealand. *Bull. Geol. Soc. Am.,* 94:791–797.

Hollister, C.D., and McCave, I.N., 1984. Sedimentation under deep-sea storms. *Nature,* 309:220–225.

Hornibrook, N. de B., and Jenkins, D.G., 1994. DSDP 594, Chatham Rise, New Zealand—Late Neogene planktonic foraminiferal biostratigraphy revisited. *J. Micropalaeontol.,* 13:93–101.

Komar, P.D., 1969. The channelized flow of turbidity currents with application to Monterey deep-sea fan channel. *J. Geophys. Res.,* 74:4544–4558.

Lawver, L.A., and Gahagan, L.M., 1994. Constraints on timing of extension in the Ross Sea region. *Terra Antarct.,* 1:545–552.

Lean, C.M.B., and McCave, I.N., 1998. Glacial to interglacial mineral magnetic and palaeoceanographic changes at Chatham Rise, SW Pacific Ocean. *Earth Planet. Sci. Lett.,* 163:247–260.

Martini, E., 1971. Standard Tertiary and Quaternary calcareous nannoplankton zonation. *In* Farinacci, A. (Ed.), *Proc. 2nd Int. Conf. Planktonic Microfossils Roma:* Rome (Ed. Tecnosci.), 2:739–785.

Matsuoka, H., and Okada, H., 1989. Quantitative analysis of Quaternary nannoplankton in the subtropical northwestern Pacific Ocean. *Mar. Micropaleontol.,* 14:97–118.

McIver, R.D., 1975. Hydrocarbon occurrences from JOIDES Deep Sea Drilling Project. *Proc. Ninth Petrol. Congr.,* 269–280.

Menard, H.W., 1955. Deep-sea channels, topography and sedimentation. *AAPG Bull.,* 39:236–255.

Meynadier, L., Valet, J.-P., and Shackleton, N.J., 1995. Relative geomagnetic intensity during the last 4 m.y. from the equatorial Pacific. *In* Pisias, N.G., Mayer, L.A., Janecek, T.R., Palmer-Julson, A., and van Andel, T.H. (Eds.), *Proc. ODP, Sci. Results,* 138: College Station, TX (Ocean Drilling Program), 779–795.

Morley, J.J., and Hays, J.D., 1979. *Cycladophora davisiana:* a stratigraphic tool for Pleistocene North Atlantic and interhemispheric correlation. *Earth Planet. Sci. Lett.,* 44:383–389.

Müller, P.J., 1977. C/N ratios in Pacific deep sea sediments: effect of inorganic ammonium and organic nitrogen compounds sorbed by clays. *Geochim. Cosmochim. Acta,* 41:765–776.

Naish, T.R., Abott, S.T., Alloway, B.V., Beu, A.G., Carter, R.M., Edwards, A.R., Journeaux, T.D., Kamp, P.J.J., Pillans, B.J., Saul, G., and Woolfe, K.J., 1998. Astronomical calibration of a southern hemisphere Plio-Pleistocene reference section, Wanganui Basin, New Zealand. *Quat. Sci. Rev.,* 17:695–710.

Neil, H.L., 1991. Late Quaternary stratigraphy, sedimentology and evolution of the Bounty Fan system, Bounty Trough, Southwest Pacific [M.Sc. thesis]. Univ. of Waikato, New Zealand.

Nelson, C.S., Cooke, P.J., Hendy, C.H., and Cuthbertson, A.M., 1993. Oceanographic and climatic changes over the past 160,000 years at Deep Sea Drilling Project Site 594 off southeastern New Zealand, Southwest Pacific Ocean. *Paleoceanography,* 8:435–458.

Normark, W.R., Hess, G.R., Stow, D.A.V., and Bowen, A.J., 1980. Sediment waves on the Monterey fan levee: a preliminary physical interpretation. *Mar. Geol.,* 37:1–18.

Pemberton, S.G., and MacEachern, J.A., 1995. The sequence stratigraphic significance of trace fossils: examples from the Cretaceous Foreland Basin of Alberta, Canada.

In Van Wagoner, J.C., and Bertram, G.T. (Eds.), *Sequence Stratigraphy of Foreland Basin Deposits*. AAPG Mem., 64:429–475.

Pemberton, S.G., van Wagoner, J.C., and Wach, G.D., 1992. Ichnofacies of a wave-dominated shoreline. *In* Pemberton, S.G. (Ed.), *Applications of Ichnology to Petroleum Exploration: A Core Workshop*. SEPM Core Workshop, 17:339–382.

Pillans, B.J., Kohn, B.P., Berger, G., Froggatt, P., Duller, G., Alloway, B.V., and Hesse, P., 1996. Multi-method dating comparison for mid-Pleistocene Rangitawa Tephra, New Zealand. *Quat. Sci. Rev.,* 15:641–653.

Pillans, B.J., Roberts, A.P., Wilson, G.S., Abbott, S.T., and Alloway, B.V., 1994. Magnetostratigraphic, lithostratigraphic and tephrostratigraphic constraints on lower and middle Pleistocene sea-level changes, Wanganui Basin, New Zealand. *Earth Planet. Sci. Lett.,* 121:81–98.

Raffi, I., and Flores, J.-A., 1995. Pleistocene through Miocene calcareous nannofossils from eastern equatorial Pacific Ocean. *In* Pisias, N.G., Mayer, L.A., Janecek, T.R., Palmer-Julson, A., and van Andel, T.H. (Eds.), *Proc. ODP, Sci. Results,* 138: College Station, TX (Ocean Drilling Program), 233–286.

Raine, J.I., Strong, C.P., and Wilson, G.J., 1993. Biostratigraphic revision of petroleum exploration wells, Great South Basin, New Zealand. *Inst. Geol. Nucl. Sci., Sci. Rep.,* 93/32.

Sato, T., and Kameo, K., 1996. Pliocene to Quaternary calcareous nannofossil biostratigraphy of the Arctic Ocean, with reference to late Pliocene glaciation. *In* Thiede, J., Myhre, A.M., Firth, J.V., Johnson, G.L., and Ruddiman, W.F. (Eds.), *Proc. ODP, Sci. Results,* 151: College Station, TX (Ocean Drilling Program), 39–59.

Spencer-Cervato, C., Thierstein, H.R., Lazarus, D.B., and Beckmann, J.-P., 1994. How synchronous are Neogene marine plankton events? *Paleoceanography,* 9:739–763.

Stam, B., Gradstein, F.M., Lloyd, P., and Gillis, D., 1987. Algorithms for porosity and subsidence history. *Computers and Geosci.,* 13:317–349.

Stock, J. and Molnar, P., 1987. Revised history of early Tertiary plate motion in the south-west Pacific. *Nature,* 325:495–499.

Suess, E., von Huene, R., et al., 1988. *Proc. ODP, Init. Repts.,* 112: College Station, TX (Ocean Drilling Program).

Takayama, T., 1993. Notes on Neogene calcareous nannofossil biostratigraphy of the Ontong Java Plateau and size variations of *Reticulofenestra* coccoliths. *In* Berger, W.H., Kroenke, L.W., Mayer, L.A., et al., *Proc. ODP, Sci. Results,* 130: College Station, TX (Ocean Drilling Program), 179–229.

Van Dissen, R., and Yeats, R.S., 1991. Hope Fault, Jordan Thrust, and uplift of the Seward Kaikoura Range, New Zealand. *Geology,* 19:393–396.

Weaver, P.P.E., Carter, L., and Neil, H., 1998. Response of surface watermasses and circulation to late Quaternary climate change, east of New Zealand. *Paleoceanography,* 13:70–83.

Wood, R.A., Andrews, P.B., Herzer, R.H., et al., 1989. Cretaceous and Cenozoic geology of the Chatham Rise region, South Island, New Zealand. *N. Z. Geol. Basin Stud.,* 3.

Worm, H.-U., 1997. A link between geomagnetic reversals and events and glaciations. *Earth Planet. Sci. Lett.*, 147:55–67.

Figure F1. Locality map for Site 1122, showing location of seismic lines 2023 and 3034 of Figure F2A, p. 39, and F2B, p. 40.

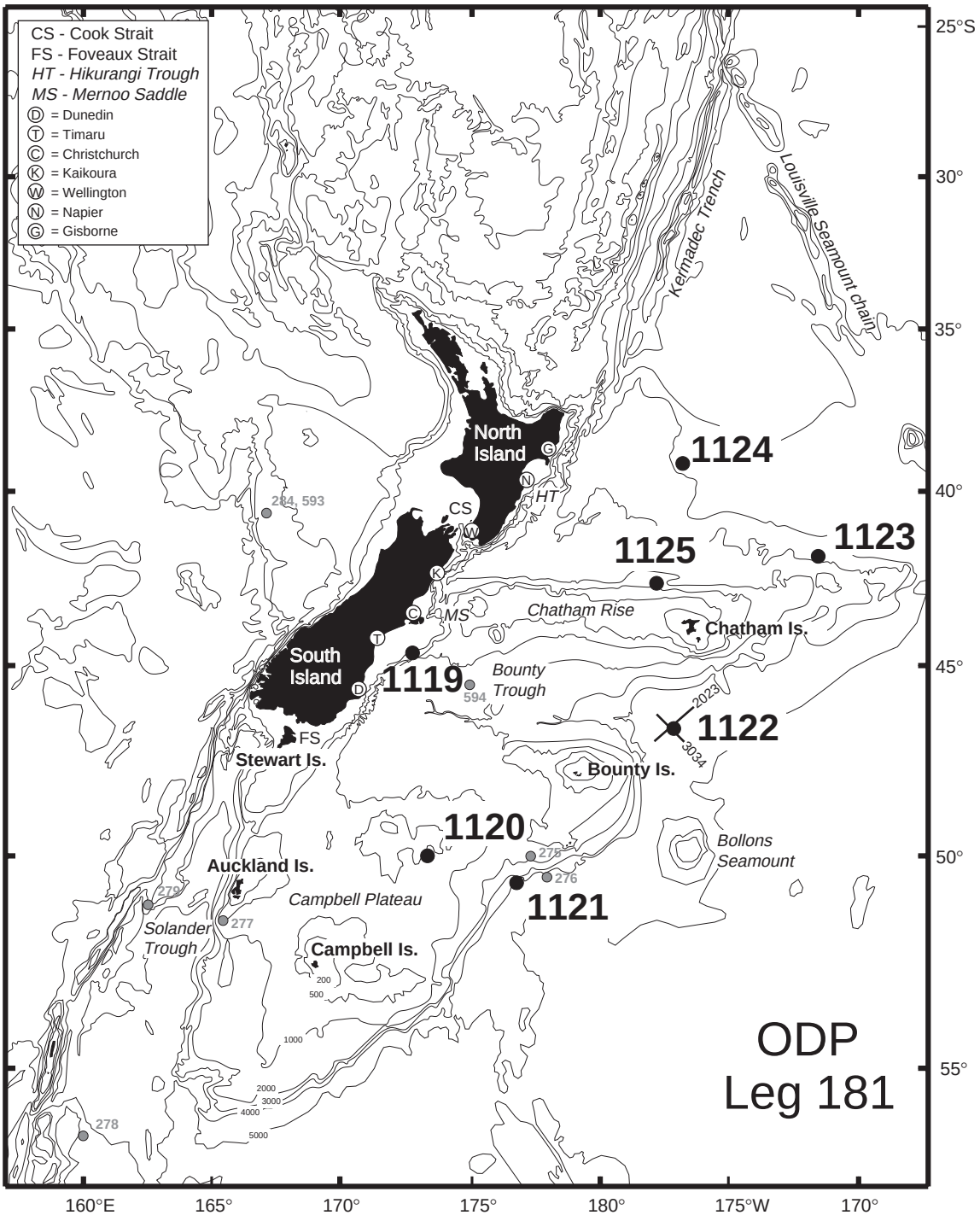

Figure F2. A. Portion of seismic line NZ01 2023 through Site 1122 (0530–1200 hr, 6 December 1998). (Continued on next page.)

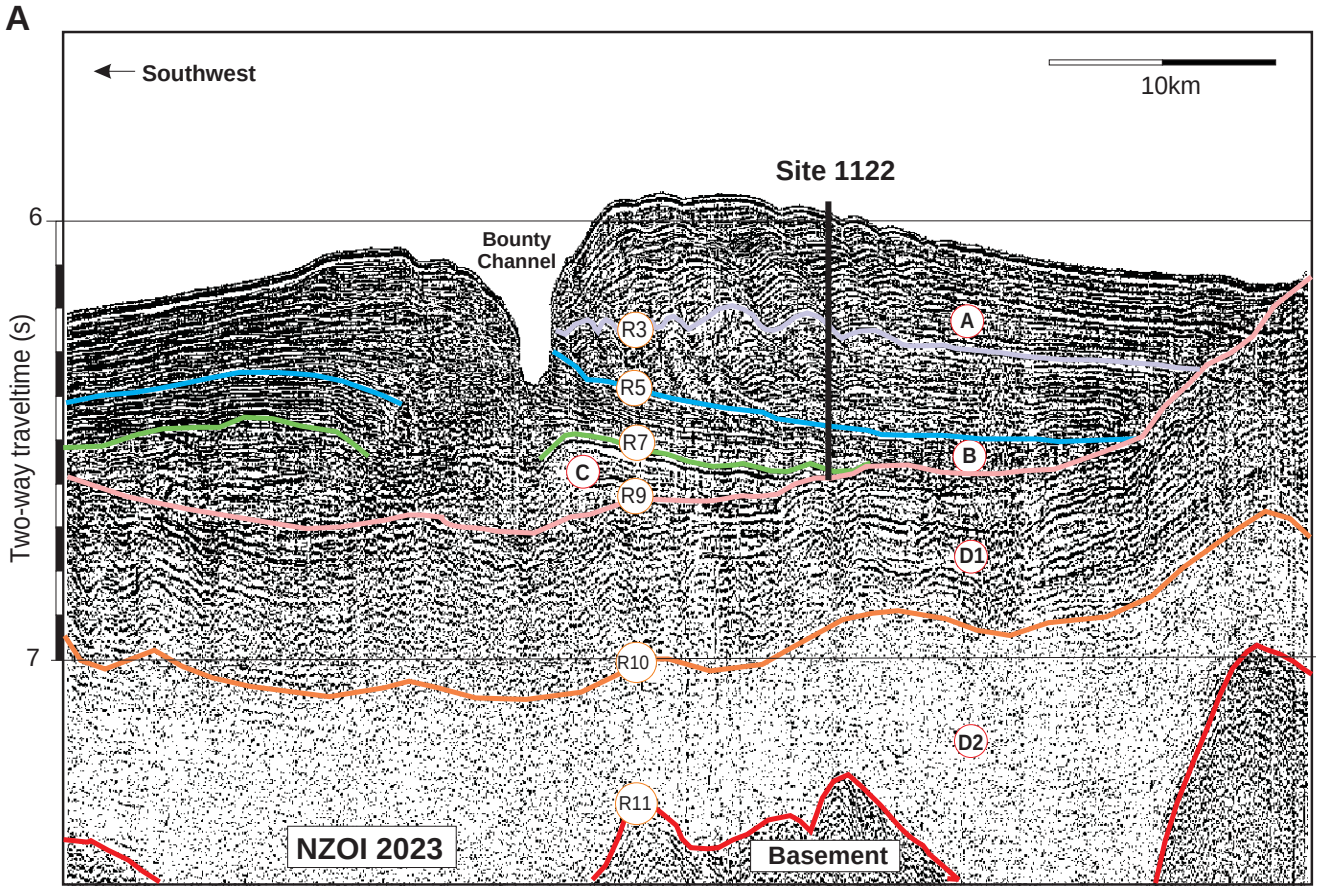

Figure F2 (continued). B. Detail of processed portion of line NIWA 3034-12 through Site 1122 (0020–0200 hr, 17 February 1997).

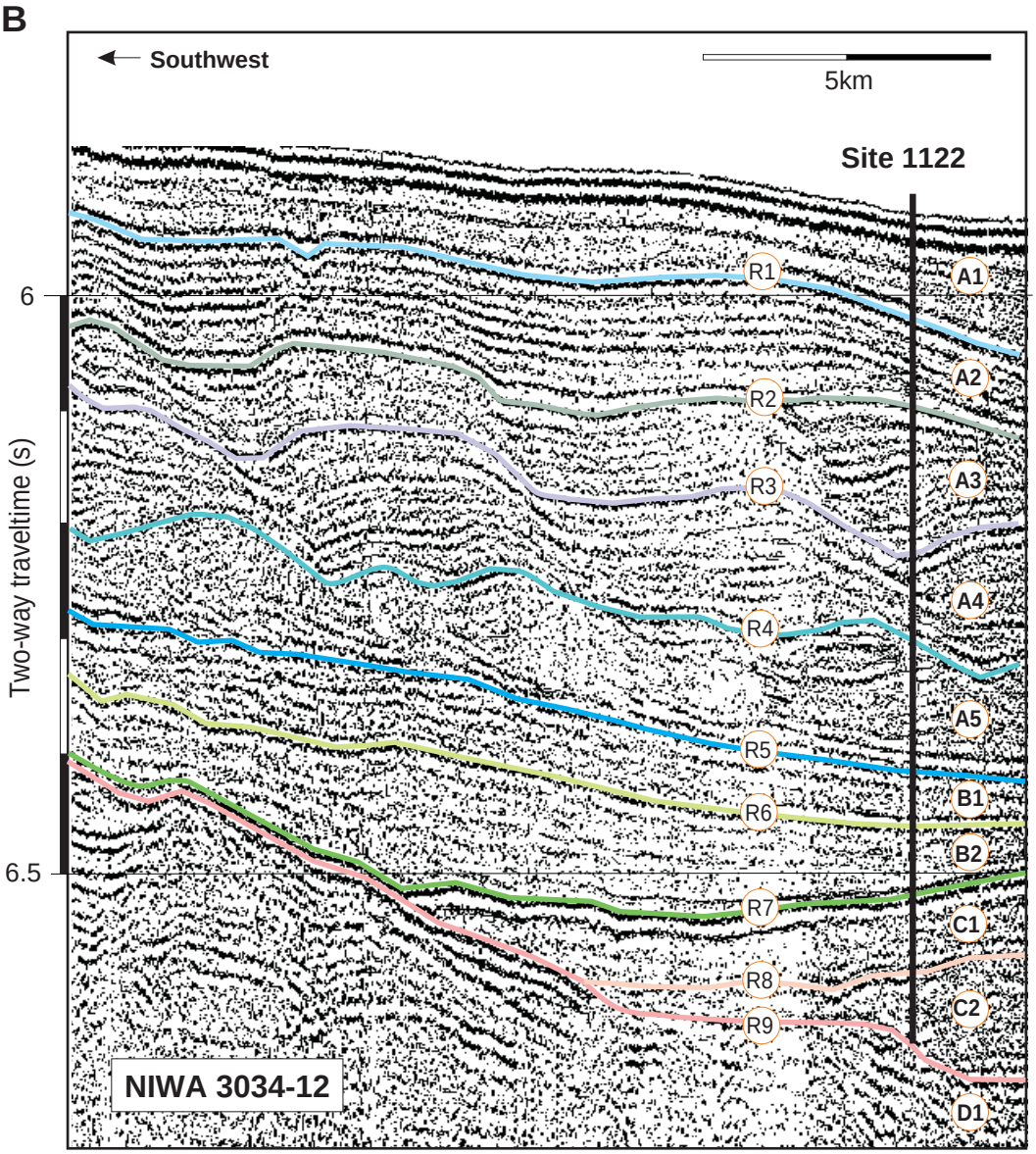

Figure F3. Portion of 3.5-kHz line NZ01 2023 through Site 1122 (0830–0940 hr, 6 December 1998).

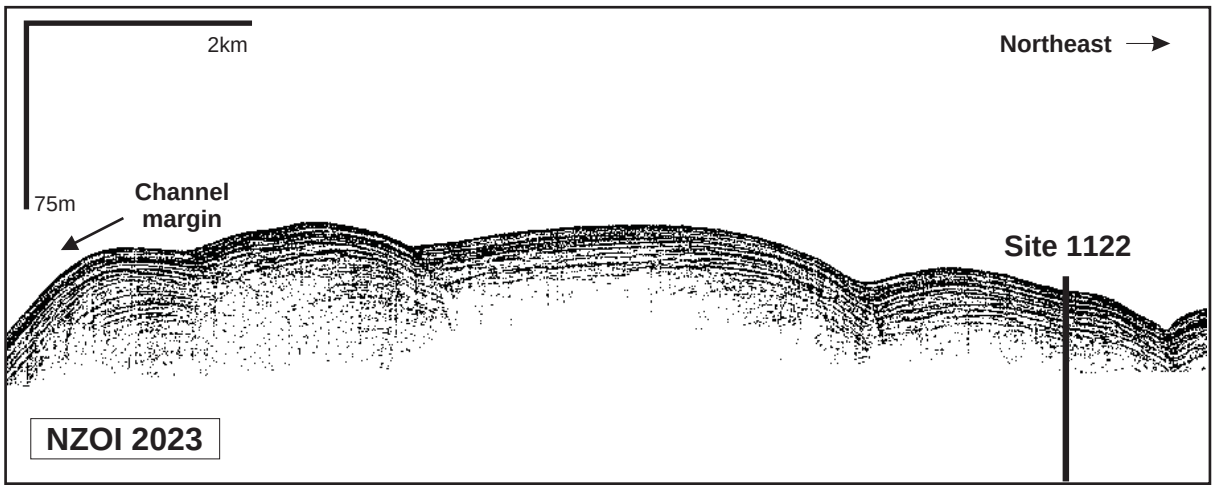

Figure F4. Summary log for Site 1122. (Continued on next three pages.)